Laser and Particle Beams (2000), *18*, 495–502. Printed in the USA.
Copyright © 2000 Cambridge University Press 0263-0346/00 $12.50

Coherence properties of high-order harmonics: Application to high-density laser–plasma diagnostic

H. MERDJI,[1] P. SALIÈRES,[1] L. LE DÉROFF,[1] J.-F. HERGOTT,[1] B. CARRÉ,[1]
D. JOYEUX,[2] D. DESCAMPS,[3] J. NORIN,[3] C. LYNGÅ,[3] A. L'HUILLIER,[3]
C.-G. WAHLSTRÖM,[3] M. BELLINI,[4] AND S. HULLER[5]

[1]Service des Photons, Atomes et Molécules, CEA-DSM-DRECAM, Centre de Saclay, 91191 Gif-sur-Yvette, France
[2]Institut d'Optique Théorique et Appliquée 91403 Orsay, France
[3]Department of Physics, Lund Institute of Technology, P.O. Box 118, S-221 00 Lund, Sweden
[4]L.E.N.S., Largo E. Fermi, 2, I-50125 Florence, Italy
[5]Centre de Physique Théorique, CNRS, Ecole Polytechnique, 91128 Palaiseau Cédex

(RECEIVED 30 August 1999; ACCEPTED 11 November 1999)

Abstract

We present two interferometry schemes in the extreme ultraviolet, based on either the wave-front division of a unique harmonic beam (1st scheme) or two spatially separated, phase-locked harmonic sources (2nd scheme). In the first scheme using a Fresnel bimirror interferometer, we measure the degree of spatial coherence of the 13th harmonic generated in xenon, as a function of different parameters. A high degree of coherence, larger than 0.5, is found for the best conditions in almost the full section of the beam. Then, we demonstrate that the second scheme can be used for interferometry measurements with an ultrahigh time resolution. The 11th harmonic is used to study the spatial variation of the electron density of a laser-produced plasma. Electronic densities higher than 2.10^{20} cm^{-3} are measured.

1. INTRODUCTION

The interaction of high-intensity laser pulses with matter produces high-density plasmas relevant to inertial confinement fusion (Milchberg *et al.*, 1988; Cable *et al.*, 1994; Levi, 1994; Workmann *et al.*, 1995) and astrophysics (Perry *et al.*, 1991; Da Silva *et al.*, 1992; Rogers & Iglesias, 1994). Optical interferometry has been widely used to study such plasmas, in particular for electron density diagnostics. However, this technique is severely restricted by free-free absorption and refraction of the optical light by the plasma. These limits constrain the measurements to low densities and plasma regions with slow density gradients. A way to overcome these limitations is to develop the interferometry technique at shorter wavelengths, typically in the soft X-ray range, where these effects can be minimized. A first demonstration in laser–plasma diagnostic was reported by Da Silva and coworkers, using a soft X-ray laser operating at 15.5 nm (Da Silva *et al.*, 1995). They probed a 1 mm long CH plasma using a Mach–Zender interferometer. More recently, electron density measurements of a colliding plasma was achieved using the same technique (Wan *et al.*, 1997). However, X-ray laser pulses are typically 50 ps long or more and cannot be used as an ultrafast diagnostic (typically subpicosecond).

Besides its fundamental interest, high order harmonic generation (HHG) has the potential to become a useful XUV source that can open new perspectives in laser–plasma diagnostic. In particular, the ultrashort pulse duration and the coherence properties are unique in the XUV range, and of obvious interest. Theobald and coworkers have taken advantage of the short harmonic pulse for measuring the time-dependent electron density of a laser produced plasma (Theobald *et al.*, 1996; Theobald *et al.*, 1999). The electron density is determined from the transmittance of the plasma at different harmonic wavelengths, respectively using the 5th and 7th orders. However, the derivation of the density from the transmittance is not really straightforward.

The coherence properties of HHG make possible to use harmonic light in interferometry. The analysis of interference patterns can directly provide, in principle, 2D map of, for example, refractive index, electron density or solid surface. Moreover, the measurements are resolved in time at the scale of ~100 fs, so that ultra short processes can be tracked. Finally, the tunability of harmonics by discrete step, over a large spectral range 100–5 nm, allows us to adapt the

Address correspondence and reprint requests to: H. Merdji, CEA, Service des Photons, Atomes et Molecules Bat. 524, Centre d'Etudes de Saclay, 91191, Gif-sur-Yvette Cedex, France. E-mail: merdji@drecam.cea.fr

https://doi.org/10.1017/S026303460018320X Published online by Cambridge University Press

probe wavelength to the spectral opacity of the plasma. The coherence of HHG can serve to interferometry in different ways. Besides the properties of spatial and temporal coherence of one single harmonic source, HHG offers the possibility of easily producing two mutually coherent (phase locked) sources, either separated in space (Zerne *et al.*, 1997) or in time (Salières *et al.*, 1999). The real, space separated, mutually coherent sources are equivalent to the Young's two-slits. The real, time separated, mutually coherent sources lead to frequency-domain interferometry in the XUV. In interferometry, the fringe shift is directly related to the electron density and a 2D map of the ionized medium can be obtained. Both schemes have been recently demonstrated as powerful subpicosecond interferometric probe for plasma diagnostics (Descamps *et al.*, 1999, Salières *et al.*, 1999).

For the space-separated sources, two schemes are relevant, according to the source are either virtual or real. In the first scheme, two secondary virtual sources S_1 and S_2 are produced from the same harmonic beam using an interferometer based on wave front division, such as Young's double-slits, Fresnel's or Lloyd's mirrors. The optics should, of course, be appropriated to the XUV range (Svatos *et al.*, 1993; Zeitoun *et al.*, 1998; Le Déroff *et al.*, 1999; Rocca *et al.*, 1999). In the second scheme, one easily produces two real harmonic sources S and S', separated in space (Zerne *et al.*, 1997), from two fundamental beams which are separately focused in the same medium.

It is of interest to compare the coherence properties which are involved respectively in the first and second interferometry schemes. Let us recall that if two rays, originated from the points P (in the beam section from source S_1 or S) and Q (in the beam section from source S_2 or S'), interfere at point M, the intensity at M involves the complex degree of mutual coherence between the vibrations from P and Q. The complex degree is defined as:

$$\gamma(P,Q;\tau) = |\gamma(P,Q;\tau)|e^{i(\alpha_{PQ}-\omega\tau)} = \frac{\langle E_P(t)E_Q^*(t-\tau)\rangle}{\sqrt{\langle|E_P|^2\rangle\langle|E_Q|^2\rangle}} \quad (1)$$

where τ is a delay introduced as an optical path difference in the interferometer (α_{PQ} is the phase of γ at zero delay).

In the first scheme, for the two sources S_1 and S_2, $P \neq Q$, and an optical delay τ much smaller than the pulse duration τ_{pulse}, one measures the degree of spatial coherence $\gamma(P,Q;0)$, for instance as a function of the distance between the two points. We will show (next study in Section 2) that a high enough degree of spatial coherence $|\gamma(P,Q;0)| \geq 0.5$ can be achieved in almost the full section of the harmonic beam (up to 3 mm), in order that an object of size $\sim$1 mm can be probed by interferometry with a good visibility of the fringes. In the case where an interferometer based on amplitude division is used, we can have $P \equiv Q$ and an optical variable delay $0 \leq \tau \leq \tau_{pulse}$. One measures then the degree of temporal coherence $\gamma(P,P;\tau)$ and the coherence time $\Delta\tau$, that is, the width of the $|\gamma(P,P;\tau)|$ function.

The second scheme offers the obvious advantage of a simple realization of the two sources S and S', from two fundamental beams, using only visible optics. In this case, the points P, Q can be said "homothetical" and are noted P, P'. The condition $\tau \ll \tau_{pulse}$ leads to measuring the degree of mutual coherence at zero delay, we note $\gamma(P,P';0)$, between the two sources. Because of the highly-controlled, coherent physics of the harmonic generation, two coherent fundamental beams of the same intensity produce mutually coherent harmonic sources. The $|\gamma(P,P';0)|$ coefficient should be therefore close to 1: the two sources are said to be "phase-locked." In practice, slightly different conditions in producing the two sources lead to a contrast of 30 to 90% in the fringe pattern. Note that the mutual coherence of the two sources at zero delay does not imply that each source should be intrinsically coherent, neither spatially nor temporally. However, by changing the delay τ between 0 and τ_{pulse}, one can also measure the $\gamma(P,P';\tau)$ function, equivalent to the $\gamma(P,P;\tau)$ under the assumption of phase-locked sources, from which the intrinsic coherence time of one source can be obtained. The configuration for an interferometry experiment, in which the object to probe should be inserted in one of the two beams, corresponds to a Young's two-slits scheme. It implies that the size of the object should not be larger than $SS' \sim 100\ \mu$m.

In this paper, we first report in Section 2 an experimental study of the spatial coherence properties of the high order harmonic, using Fresnel's mirrors interferometer (first scheme). Among the applications of the HHG, interferometry in the XUV range serving to plasma diagnostic appears very promising. To demonstrate its feasibility, we report in Section 3 an interferometry experiment using two space-separated phase locked sources (second scheme), in which we have measured the electron density of a laser produced plasma.

2. SPATIAL COHERENCE PROPERTIES OF HIGH-ORDER HARMONICS

At first sight, the spatial coherence of the harmonics is expected to be high since it should reflect that of the laser field. The spatial and temporal coherence properties have been studied revealing the complex underlying physics of high-order harmonic generation (Ditmire *et al.*, 1996; Bellini *et al.*, 1998; Le Déroff *et al.*, 1999; Lyngå *et al.*, 1999). From a fundamental point of view, the coherence properties involve the detailed history of the time- and space-dependent nonlinear polarization which vary differently in time at different places in the medium. As a result, the fields produced at the two points P and Q at the end of the medium will build up through different histories and might subsequently show a reduced degree of coherence $|\gamma(P,Q;0)|$. The spatial coherence of high harmonics has been thoroughly studied in a Young's two-slits experiment by Ditmire and coworkers (Ditmire *et al.*, 1996; Ditmire *et al.*, 1997). They have reported that the coherence degree of the 11th to 19th harmonic near-

https://doi.org/10.1017/S026303460018320X Published online by Cambridge University Press

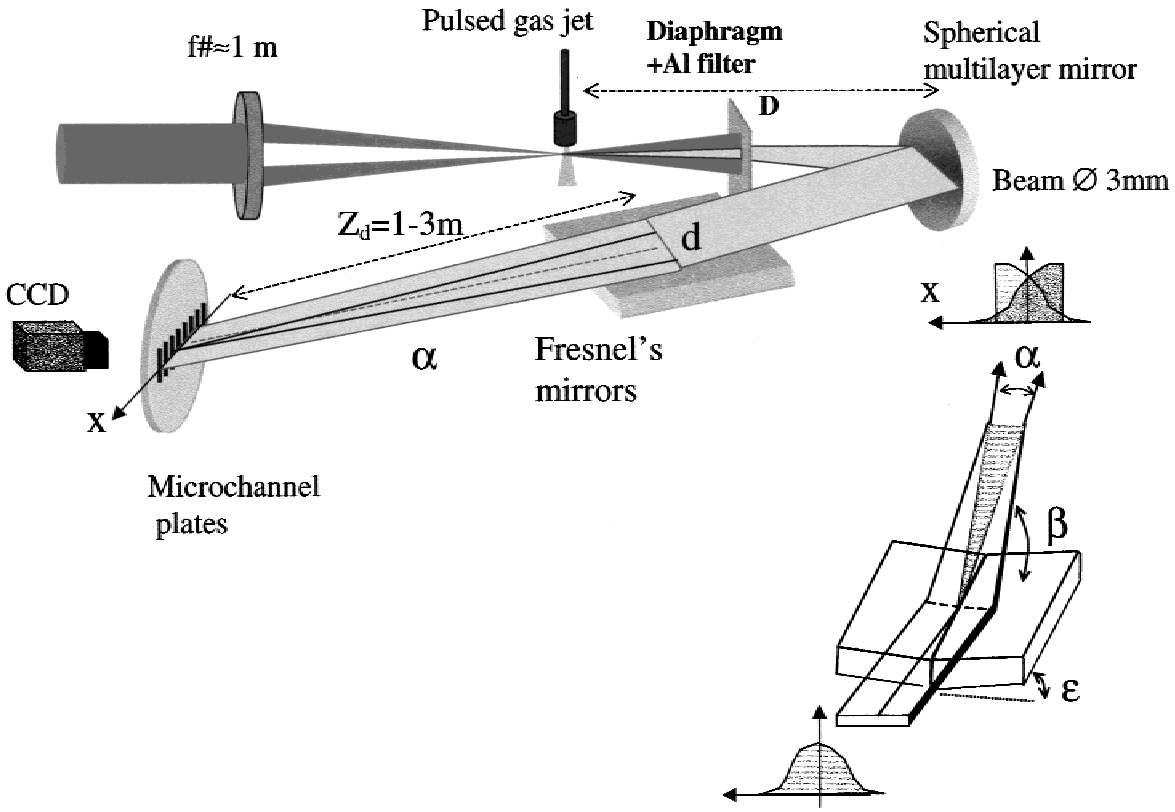

Fig. 1. Experimental set-up showing the annular laser beam, diaphragm and Al filter, multilayer mirror, Fresnel's mirrors interferometer, and microchannel plate detector. The detector is tilted to increase the resolution.

field can be larger than 0.5, within coherence cell of diameter up to 15% of the full beam diameter. Moreover, they have shown that the coherence is degraded as the atomic density, and consequently the electron density produced by ionization, is increased. Indeed, the electron density produced by laser ionization of the generating medium is a time- and space-dependent factor which can chirp the fundamental beam, affect phase matching and the harmonic field propagation, leading to a lower correlation of the fields in two different points at the medium exit.

In our experiment carried out at the femtosecond LUCA laser facility of CEA/DRECAM in Saclay, we have used an interferometer of the Fresnel's mirrors type to study the coherence of the 13th harmonic (H13) produced in xenon, over the full section of the harmonic beam. The main differences with the study by Ditmire *et al.* (1997) are discussed in the following description of the experimental set-up and results. The experimental set-up is shown in Figure 1. A ring shaped IR beam (<10 mJ at 800 nm; 60 fs; 20 Hz; numerical aperture $r/f \approx 1/200$) is focused to an intensity of 10^{13}–10^{14} W/cm^2 in a xenon gas jet, then cut on a diaphragm when it diverges, in order that only the harmonics emitted on axis are transmitted. At a distance $D = 1.3$ m from the source, we use a Mo/Si multilayer mirror and a self-supported 100 nm-thick aluminum foil to effectively select the 13th and 15th harmonics. The beam reflected towards the interferometer is parallel, with a rather regular, close to Gaussian, spatial distribution of intensity, the full width at $1/e^2$ being around 3 mm. The Fresnel's mirrors consist of two plane, silica half-mirrors, which are tilted around their common straight edge (Svatos *et al.*, 1993). The harmonic beam, incoming parallel to and centered on the mirror ridge, is reflected at grazing incidence on the two half-mirrors, in order that the two reflected half-beams cross and overlap under an angle $\alpha \approx 1$ mrad, generating an interference pattern. With this geometry, the rays that interfere at a given distance Z_d after the interferometer are all the pairs, respectively at P and Q in the transverse section of the incident beam, such that, (1) P and Q are horizontally aligned, and (2) P, Q are separated by $d = \alpha Z_d < 3$ mm. A 2D-interferogram is measured at distance Z_d from the interferometer on a single shot detector. It can be read as a map of the spatial coherence throughout the beam, for a fixed distance d between all the interfering rays. This makes the technique more straightforward than the Young's two-slits separated by d since, in the latter scheme, a complete mapping of the coherence requires that the slits are moved throughout the beam section, thus excluding any single shot measurement. With the Fresnel's mirrors setup, the distance d is easily changed by simply varying the distance Z_d between the interferometer and the detector. By changing Z_d between 1 and 3 m, we probe the transverse coherence of the beam at different distances $d = 1$ to 3 mm.

https://doi.org/10.1017/S026303460018320X Published online by Cambridge University Press

The fringe spacing $i = \lambda/\alpha \approx \lambda Z_d/d$ (60 μm for H13) depends only on the wavelength, so that the interferograms can be measured with the same resolution. As a drawback, this technique introduces diffraction by the mirror central edge. The detector is a CsI coated, two-microchannel plates assembly, coupled to a phosphor screen on which the fringe pattern is imaged with a CCD camera. The overall spatial resolution of 90 μm makes it necessary to tilt the detector, so that the effective fringe spacing is multiplied by 7 on the channel plates.

Figure 2 shows a 2D-interferogram measured for Z_d = 2 m, that is, $d = 2$ mm, a pressure of 100 Torr in the jet and a position $z = +80$ mm of the jet relative to the laser focus ($z > 0$ for a laser focused before the jet; the medium length of 1 mm is small compared to the confocal parameter 50 mm). The almost symmetrical envelope of the distribution corresponds to the two crossed, half-Gaussian beams. Well contrasted fringes are superimposed where the half-beams overlap, indicating a good spatial coherence at the scale of d. Note that in Figure 2, we have performed a spatial frequency filtering in the Fourier space to remove the 15th harmonic (causing a beat modulation when superimposed with the 13th harmonic fringe pattern). By the same technique, we can resolve the diffraction by the central mirror edge from the interference modulation (Le Déroff *et al.*, 1999). After analysis, we obtain the local degree of spatial coherence $|\gamma_d(P,Q;0)|$ for the 13th harmonic. In most cases, it appears rather uniform throughout the beam section: in the case of Figure 2, it fluctuates around 0.6. We finally derive a mean value $\gamma_d = \langle|\gamma_d(P,Q;0)|\rangle$, averaged over the (P,Q) pairs in the beam section. For the best conditions of focussing and pressure, we obtain $\gamma_d = 0.8, 0.6, 0.4$ within a $\pm$ 0.1 uncertainty, for respectively $d = 1$, 2 and 3 mm. This means that the coherent flux is almost equal to the total harmonic flux. Therefore, the interferometry scheme with a large coherent beam should allow probing large size object. Obviously, the measured γ_d is much larger than the one of the far-field produced from an incoherent source like X-ray lasers (Da Silva *et al.*, 1995; Zeitoun *et al.*, 1998; Rocca *et al.*, 1999), and actually, it corresponds to the intrinsic coherence of the 13th harmonic near-field. According to the van Cittert–Zernike theorem (Born & Wolf, 1980), the light emitted from a purely incoherent source of radius ρ will present a given degree of coherence, say $\gamma_d \geq 0.6$, within a cell of diameter $d = d_{incoh}$, which increases with the distance D from the source as $d_{incoh} = 0.2\lambda D/\rho$. Using an estimated size $\rho \sim 100$ μm for the harmonic source radius, the distance $D = 1.3$ m, we find that the coherence cell has a diameter $d_{incoh} \approx 160\,\mu$m, much smaller than the distance $d = 2$ mm for which the same degree of correlation is measured in the harmonic beam. However, note from the above discussion that, rather than the intrinsic coherence, the brilliance of the source (number of photons/s/unit of source area/unit of solid angle/fraction of bandpass) should be the effective parameter for discussing its practical use in an interferometry experiment. To that respect, X-ray laser compensate their poor intrinsic coherence by a high brilliance.

As already reported by Ditmire and coworkers, we have found that the γ_d decreases as the atomic density is increased, due to the onset of time- and space-dependent electron density as ionization develops in the medium. In Figure 3, we show the variation of the γ_d as a function of the position z of the jet relative to the laser focus. For a fixed pressure of 100 Torr in the jet, $d = 2$ mm, γ_d increases from 0.3 when the laser beam is focused in the jet, to 0.7 when the laser focus is at $z = 100$ mm before the jet and the harmonic signal close to its maximum value. The observed variation should partially reflect the higher ionization which develops in the focus region, leading to a degraded spatial coherence as above mentioned. However, we claim that it mainly reflects the effect of the intensity-dependent, that is time- and space-dependent phase of the nonlinear polarization (Salières *et al.*, 1995). To prove this statement, we have performed complete simulations of the 13th harmonic in the far-field (Strong Field Approximation), and computed γ_d as a function of z for different pressures in the medium (L'Huillier *et al.*, 1992). The computed γ_d is shown in Figure 4. It decreases from 1 when the laser is focused either far before or far after the jet, to 0.6 when the focus is at 20 to 30 mm after the jet. The calculated γ_d in Figure 4 are at least in qualitative agreement with the experimental points: they both de-

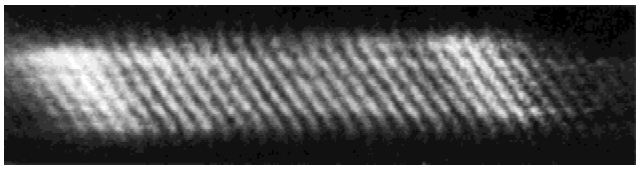

Fig. 2. 2D interferogram of 13th harmonic beam, measured at distance Z_d = 2 m, that is, for a distance $d = 2$ mm between the interfering rays in the incident beam, $P = 100$ Torr in the jet and a position $z = +80$ mm of the jet relative to the laser focus. The spatial frequency associated to the 15th harmonic has been removed by filtering in the Fourier space.

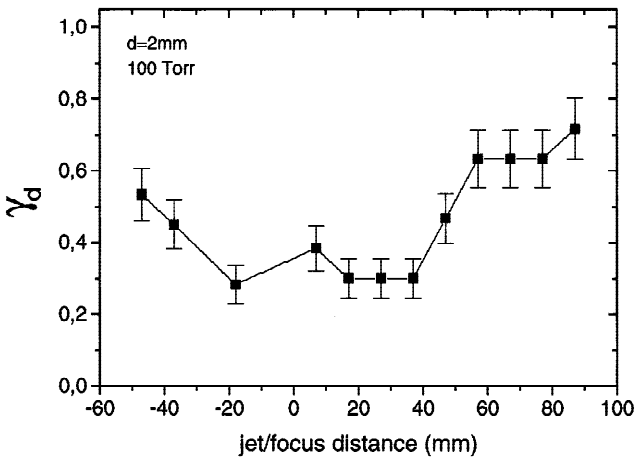

Fig. 3. Degree of spatial coherence for $d = 2$ mm, measured as a function of the relative jet-to-focus position ($z > 0$ for focus before the jet).

https://doi.org/10.1017/S026303460018320X Published online by Cambridge University Press

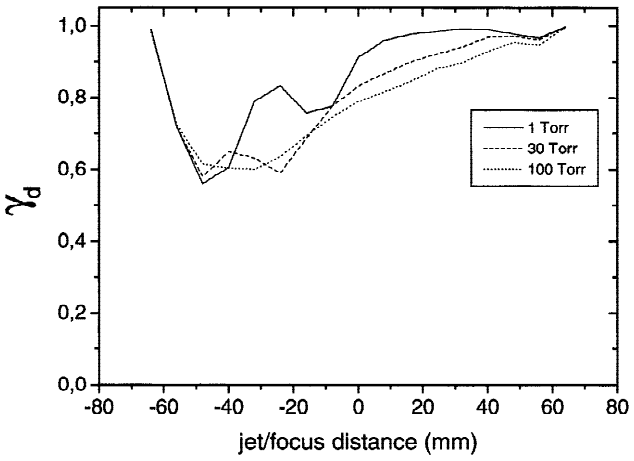

Fig. 4. Degree of spatial coherence for $d = 2$ mm, calculated as a function of the jet-to-focus position for three different pressures. Coherence is minimum when the focus is close to the jet, even at very low pressure (1 Torr, electron density negligible). This indicates that coherence should be degraded through the intensity-dependent phase of the atomic dipole.

crease to a minimum when the jet is close to the focus. The calculated γ_d exhibits a pronounced asymmetry with respect to focussing in the jet ($z = 0$), for the three pressures considered. The asymmetry means that the nonsymmetrical phase of the nonlinear polarization (and nonsymmetrical phase-matching) should be involved. The asymmetry is much less visible on the experimental points. The experimental minimum extends over a larger z region; it is lower (0.3) than the calculated one. The obvious discrepancies between computed and experimental points can be attributed, on the one hand, to the large uncertainty (± 10 mm) on the absolute origin (focus position) in Figure 3. On the other hand, the simulations use a Gaussian laser beam whereas it is experimentally close to Gaussian but with a beam quality factor $M^2 = 2$. As a result, the region of the jet close to focus, where the dependence of the harmonic field with the fundamental is the most critical, may not be well enough described in the simulations. However, we think that the simulations prove the following important point: even at very low pressure (1 Torr), when the electron density plays no role, the degree γ_d shows a marked decrease in the focus region which can only be attributed to the intensity-dependent, intrinsic dipole phase in the nonlinear polarization. At higher pressure, the calculated variation is very close to the one with negligible electron density. Therefore, the intrinsic phase still mainly determines the coherence degree, the contribution of the electron density being limited.

3. APPLICATION OF HIGH-ORDER HARMONICS TO HIGH-DENSITY LASER-PLASMA DIAGNOSTICS

In this section, we report the successful application of high order harmonic in XUV interferometry, namely to the dynamical study of a dense plasma in the subpicosecond regime. As we recall in the Introduction, Zerne and coworkers have shown that two real, phase-locked harmonic sources, separated in space, can be generated from the same laser. This scheme we call the second scheme has the advantage of avoiding use of XUV mirrors, in particular of XUV beam splitters, which are extremely difficult to produce in this spectral range.

The experiment was carried out at the Lund High-Power Laser Facility. The set-up is similar to the one previously used to characterize the temporal coherence properties of high order harmonics (Bellini *et al.*, 1998; Lyngå *et al.*, 1999). A titanium-sapphire laser system delivers pulses at 790 nm, of 200 mJ, 110 fs duration, at a repetition rate of 10 Hz. Then, two pulses of equal intensity are produced in a Michelson interferometer. The two beams are focused under numerical aperture $r/f = 1/100$ into a pulsed krypton gas jet. The energy is about 0.5 mJ for each pulse, which leads to a peak intensity of the order of 10^{14} W/cm^2 at the focus. In order to produce two spatially separated foci in the medium, one arm of the Michelson interferometer is slightly misaligned. The two harmonic sources are thus real and typically separated by 130 μm, the configuration being equivalent to the Young's two-slits. After propagation, the two diverging, mutually coherent beams overlap and interfere in the far field. The visibility of the fringes is better than 30%. The harmonics are spectrally analyzed with a normal incidence spherical ($R = 1$ m) grating with 1200 lines/mm. The interference pattern is measured on microchannel plates coupled to a phosphor screen. The images are then digitized by a 16-bit CCD camera.

The feasibility of the method has been first demonstrated by probing phase shifts induced by a thin aluminum foil. The interferograms exhibit fringe shifts varying with the harmonic order (from 9th to 15th) from which the thickness of the foil can be determined. In this section, we focus on a further application, in which we have measured the electron density in a laser-produced plasma on a solid target. The plasma is produced by irradiating a 50-μm thick aluminum foil fixed on a flat glass support with a 300 ps, 790 nm, laser pulse (pump) focused to an intensity of a few 10^{13} W/cm^2. The plasma is probed 1.2 ns after its production: one harmonic beam passes through the expanding medium and is phase shifted, whereas the second beam propagates in vacuum without perturbation. At the probe time, hydrodynamic expansion and recombination have already occurred and the electron density of the plasma is typically ranging from 10^{20} to a few 10^{22} cm^{-3}. The irradiated target is located 25 mm after the focus of the one laser beam generating the harmonics, so that the beam has diverged enough and does not perturb the plasma. The velocity of the ablated material is about 10^7 cm/s. We estimate that the plasma size is approximately 100 μm at the time we probe it; it is slightly larger than the harmonic beam size of about 70 μm. In order to keep a phase reference, the two harmonic sources (probe and reference) are aligned at 45° relative to the target plane. In our case,

https://doi.org/10.1017/S026303460018320X Published online by Cambridge University Press

100 μm is an upper limit of the typical dimensions that can be probed.

Figure 5 shows a radiography of the plasma, using the 7th harmonic (113 nm) as a probe beam. This technique is similar to X-ray shadowgraphy with the point projection method (Yamanaka *et al.*, 1982). It allows us to check how the harmonic probe is perturbed across the ionized medium. The image in Figure 5 shows that the self-emission of the plasma is not strong enough to fully override the harmonic beam print on the detector. In absence of the plasma, the harmonic beam profile is close to Gaussian. With the plasma, the transmitted light is strongly reduced in the most dense regions, where absorption or refraction take place. At wavelength $\lambda = 113$ nm, the critical electron density is equal to 8–10^{22} electrons/cm^3; it is one order of magnitude higher than the typical densities of the plasma. Bremsstrahlung absorption is therefore negligible in our conditions. Bound-free or bound-bound absorption of multicharged ions are the most probable processes at the origin of the beam attenuation observed in Figure 5.

In Figure 6, we show single shot interference pattern obtained with the two 7th harmonic probe beams and with plasma present, in the same conditions as in radiography in Figure 5. The initial target surface is approximately indicated in the figure. We first observe that the harmonic is perturbed at the same position as in Figure 5. In the upper part of the image, the interference pattern has completely disappeared due to atomic absorption of the harmonic beam. In the lower part, the fringes are tilted compared to a vertical reference (without plasma). Because of absorption it is difficult to make reliable density measurements out of the data with the 7th harmonic.

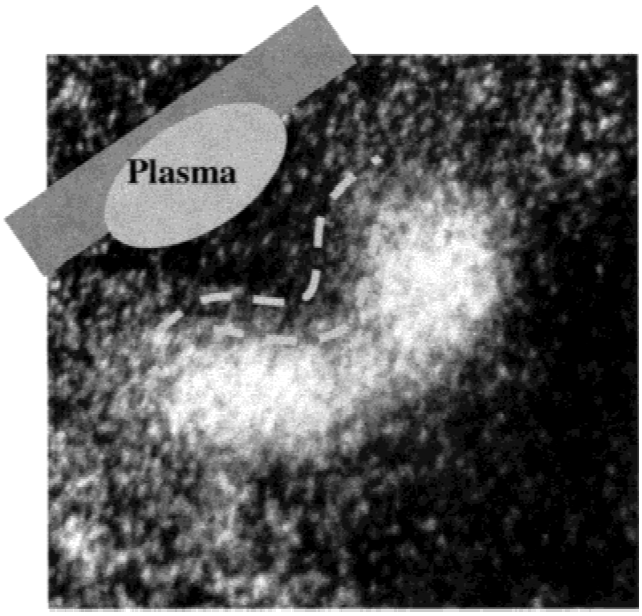

Fig. 5. Single shot XUV radiography of the aluminum plasma using one 7th harmonic probe beam. The position of the plasma is shown in the figure. The dashed lines sketch the expanding plasma.

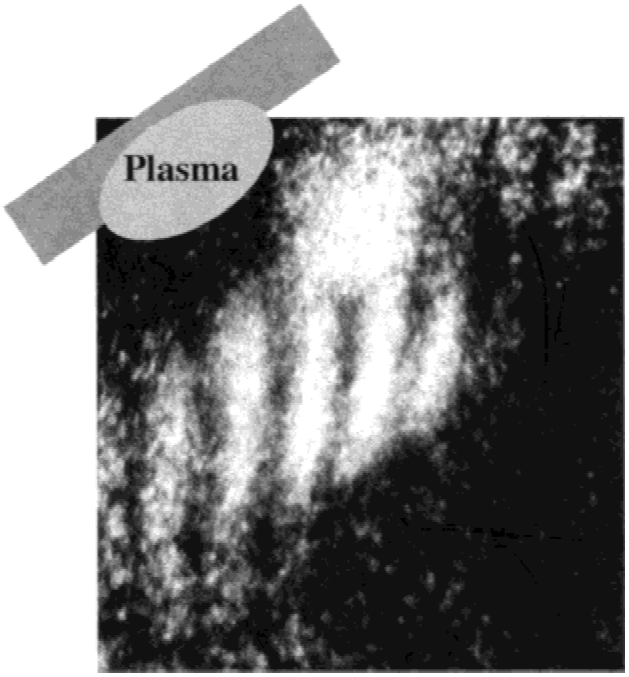

Fig. 6. Single shot interference pattern of the two 7th harmonic probe beams, with plasma present. Distortion of the fringes are clearly visible.

Now, the harmonic wavelength can be easily tuned to a higher, less absorbed order, by simply tuning the spectrometer. For example, the interference patterns recorded with the 11th harmonic (72 nm) are presented in Figure 7. In this case, the harmonic probe beam is not absorbed or refracted by the plasma, as also confirmed by radiography measurements. In Figure 7a, without plasma, the interference pattern presents a good fringe visibility. When the plasma is produced (Figure 7b and c), we still clearly distinguish the fringe pattern. The noise level has increased compared to Figure 6, which is probably due to the presence of more Al emission lines in this spectral range. The shift of the fringes reveals the presence of high density plasma close to the initial target surface. The shift is quite regular indicating that the plasma is rather homogeneous at the probe time. The number N of fringe shift at a wavelength λ is given by

$$N = \int_0^d \frac{1 - n_{ref}}{\lambda}\, dx \approx \frac{L}{2\lambda}\,\frac{N_e}{N_c}, \qquad (2)$$

where:

$n_{ref} = \sqrt{1 - N_e/N_c}$ = plasma refractive index,

and where the integral is taken over the plasma length $L \sim 100$ μm, assuming that refraction effects are negligible. In Figure 7b, the harmonic probe beam is not fully embedded in the plasma so that we observe unperturbed fringes aside the plasma, far away from the target. Assuming that the plasma is uniform along the probe path, we have a useful reference which can be used to map the electron density in

https://doi.org/10.1017/S026303460018320X Published online by Cambridge University Press

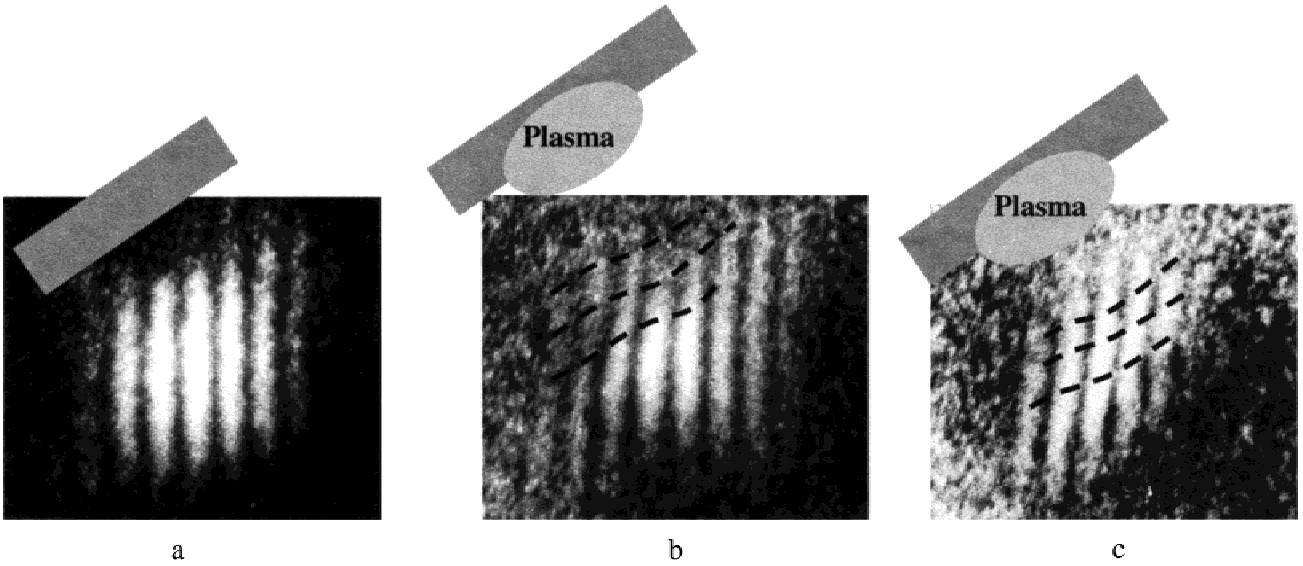

Fig. 7. Single shot interference pattern recorded using the 11th harmonic (a) without; (b) and (c) with plasma. The position of the plasma is shown in the figure, together with iso-density lines (dashed lines).

the two dimensions of the expansion. In Figure 7b, we have plotted some iso-density lines; they reveal that the hydrodynamic expansion of the plasma is mainly perpendicular to the target plane. We measure densities ranging from $9 \cdot 10^{19}$ cm^{-3} (line at bottom) to $2 \cdot 10^{20}$ cm^{-3} (line at top). In Figure 7c, the fringes are tilted in the whole interference field so that we do not have any reference. If we take as a reference the position of the fringes at the bottom of the image, we measure a minimum fringe shift of 0.8, corresponding to an electron density of at least $2.5 \cdot 10^{20}$ cm^{-3}. In Figure 8, we have plotted the electron density profiles at different times Δt of the plasma expansion, computed with

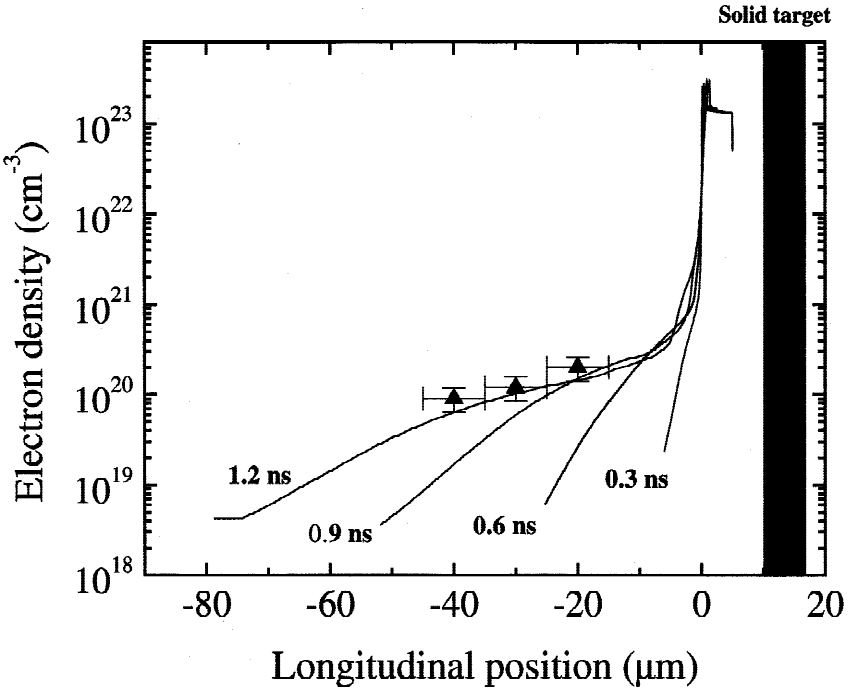

Fig. 8. Solid lines: Simulations of electron density profiles at different delays between plasma creation and probe beam of the plasma expansion, using the MULTI hydro-radiative code with parameters λ_{pump} = 800 nm, t_{pump} = 300 ps (FWHM), and $I_{pump} = 3 \cdot 10^{13}$ W/cm^2. Triangle: experimental points from image 7b.

https://doi.org/10.1017/S026303460018320X Published online by Cambridge University Press

the MULTI 1D hydro-radiative code (Ramis 1988). The experimental points at $\Delta t = 1.2$ ns, measured from the interferogram in Figure 7b, are also shown. The agreement is quite good and confirms the experimental observation of a quite homogeneous plasma with linear gradients.

4. CONCLUSION

We have reported two interferometry experiments in the XUV range, which both involve the coherence properties of high harmonic generation in gas, from a Ti:Sa laser at 800 nm.

First, we use Fresnel's mirrors interferometer to produce two harmonics sources by wavefront division of the harmonic beam, and to study its spatial coherence. With this scheme, we can measure a 2D map of the degree γ_d of spatial coherence, for a given distance d between the interfering rays in the transverse section of the incident beam. As expected, the harmonic beam presents a relatively high spatial coherence. For example, we measure an average degree $\gamma_d \geq 0.5$ in coherence cell of diameter $d = 2$ mm, close to the beam diameter: the coherent flux is almost equal to the total flux. Interferometry experiment based on wavefront division and probing large size objects is therefore possible with harmonics. The study indicates that the intensity-dependent phase of the atomic dipole should play a major role in the spatial coherence properties of harmonic emission.

Second, we use an interferometry scheme analogous to the Young's two-slits, to measure the time-dependent electron density in a laser-produced plasma on a solid target. The scheme, involving two phase-locked, space-separated harmonic sources, has the advantage of avoiding any optical XUV beam splitters. It demonstrates that subpicosecond XUV interferometry, using harmonics, is now accessible using a table-top laser. It emphasizes the advantage of having a quasitunable XUV source, to overcome absorption and refraction effects in plasma diagnostics.

The one or the other interferometry scheme can be used for time-resolved measurements in various systems. We believe that it can be particularly useful as an ultrafast plasma diagnostics, that is characterization of ultrafast processes such as, for example, the propagation of ultrashort pulses in overdense plasmas.

ACKNOWLEDGMENTS

The work carried out in Lund was supported by the European Community under contract N° ERBFMGECT950020 and N° ERBFMBICT983348, by the Swedish Natural Science Research Council and by the Göran Gustafsson's Foundation for Medicine and Natural Science.

REFERENCES

Bellini, M. *et al.* (1998). *Phys. Rev. Lett.* **81**, 297.
Born, M. & Wolf, E. (1980). (6th ed.) Cambridge University Press, p. 508.
Cable, M.D. *et al.* (1994). *Phys. Rev. Lett.* **73**, 2316.
Da Silva, L.B. *et al.* (1992). *Phys. Rev. Lett.* **69**, 438.
Da Silva, L.B. *et al.* (1995). *Phys. Rev. Lett.* **74**, 3991.
Descamps, D. *et al.,* submitted to *Opt. Lett.* in August 1999.
Ditmire, T. *et al.* (1996). *Phys. Rev. Lett.* **77,** 4756.
Ditmire, T. *et al.* (1997). *Appl. Phys.* **65**, 313.
LeDéroff *et al.,* submitted to *Phys. Rev. A* in August 1999.
Levi, B.G. (1994). *Phys. Today* **9**, 17.
L'Huillier, A. *et al.* (1992). *Phys. Rev. A* **46**, 2778.
Lyngå, C. *et al.,* submitted to *Phys. Rev. A* in May 1999.
Milchberg, R.R. *et al.* (1988). *Phys. Rev. Lett.* **61**, 2364.
Perry, T.S. *et al.* (1991). *Phys. Rev. Lett.* **67**, 3784.
Quéré, F. *et al.,* submitted to *Phys. Rev. Lett.* in June 1999.
Ramis R. *et al.* (1988). *Comput. Phys. Commun.* **49**, 475.
Rocca, J.J. *et al.* (1999). *Opt. Lett.* **24**, 420.
Rogers, F.J. & Iglesias, C.A. (1994). *Science* **263**, 50.
Salières, P. *et al.* (1995). *Phys. Rev. Lett.* **74,** 3776.
Salières, P. *et al.,* submitted to *Phys. Rev. Lett.* in August 1999.
Svatos, J. *et al.* (1993). *Opt. Lett.* **18**, 1367.
Theobald, W *et al.* (1999). *Phys. Rev. E* **59**, 3544.
Theobald, W. *et al.* (1996). *Phys. Rev. Lett.* **77**, 298.
Wan, A.S. *et al.* (1997). *Phys. Rev. E* **55**, 6293.
Workmann, J. *et al.* (1995). *Phys. Rev. Lett.* **75**, 2324.
Yamanaka *et al.* (1982). *SPIE,* **348** 783.
Zeitoun, P. *et al.* (1998). *Nucl. Instr. And Meth. A* **416**, 189.
Zerne, R. *et al.* (1997). *Phys. Rev. Lett.* **79**, 1006.

https://doi.org/10.1017/S026303460018320X Published online by Cambridge University Press